Microstructural Patterns, Microsegregation, Porosity, and Mechanical Properties of Hypoeutectic Al-Fe Alloy, and its Dependency with Solidification Thermal Parameters

Bruno Silva Dantas[a], Wysllan Jefferson Lima Garção[b], Franciele de Matos Peixoto[a],

Nilmara Almeida Guimarães[b], Ingrid Meirelles Salvino Tomaszewski[c], Alexandre Furtado Ferreira[a]*

[a]Universidade Federal Fluminense (UFF), Programa de Pós-Graduação em Engenharia Metalúrgica, 27255-125, Volta Redonda, RJ, Brasil.
[b]Instituto Federal do Rio de Janeiro (IFRJ), 27213-100, Volta Redonda, RJ, Brasil.
[c]Faculdade de Tecnologia de Cruzeiro (FATEC), 12701-170, Cruzeiro, SP, Brasil.

Al-Fe alloys are usually used as packaging and structural materials, but in the recent years, there have been considered for possible applications in aerospace field. The solidification sequence in pure aluminum containing 1 wt.% Fe is described in term of the formation of macrostructure, microstructure, microsegregation, porosity and mechanical properties. This material was studied in the upward unidirectional solidification system under transient heat flow conditions. Differences in microstructure, microsegregation, porosity and mechanical properties such as ultimate tensile strength, elongation and microhardness, due to the thermal parameter effects were observed and discussed. Experimental growth laws relating cellular spacing to the cooling rate and solidification speed have been determined, indicating that the increase in thermal parameter have induced a refinement effect on cell morphology. Microsegregation profiles of Fe solute were experimentally determined from the central region of the cell to the intercellular region under different solidification speeds. The Fe microsegregation determined from central region of the cell ($F_S = 0$) to the intercellular region ($F_S = 1$) show a growing profile, in any case considered. However, the profiles move upward with the increase in solidification speed, which indicates that Fe solubility in solid, increases with the increase in solidification speed. The effect of the solidification thermal parameters and cellular spacing on the porosity content were experimentally investigated. The value of porosity content increased along the casting. These results have pointed out that porosity content is affected by solidification parameters and cellular patterns. Further, measurable effects of the thermal parameters, cellular spacing and porosity content on the mechanical properties were experimentally determined. It stands out among experimental results the influence of porosity on the mechanical properties of as-cast material. In any case analyzed, mechanical properties increase with decreasing porosity content.

Keywords: *Aluminum alloys, solidification, alloying elements, cell microstructure and mechanical properties.*

1. Introduction

Al-Fe alloys constitute one of the commercially important classes of aluminum alloys. These alloys are used as packaging and structural materials, but in recent years, there has been a considerable amount of research on the Al-Fe-based alloys for possible applications in aerospace structure. Although these alloys are almost always subjected to secondary processing such as rolling or extrusion after the primary casting, the mechanical properties resulting from thermomechanical treatment depends on the cast microstructures. Not only the microstructural patterns itself (cells or dendrites, inclusions, intermetallic and porosity) but also the chemical arrangement (i.e., microsegregation) are closely connected to the mechanical properties non-uniformity of final product. However, because of the complexity of microstructural evolution during casting, a sequence of events (microsegregation, cooling rates, solidification speed, etc.) that governs microstructure formation can vary considerably in as-cast materials[1].

The planning of homogenization and dissolution heat treatments is dependent on the microsegregation level in as-cast materials. During these heat treatments, mass flux by diffusion is responsible for the decrease in microsegregation level, and the treatment duration is dependent on the time required to diffuse a solute over a microstructural distance, i.e., the cellular or dendrite spacing that characterizes the solidification microstructure[2].

One of the most severe types of defects found in castings, is microporosity, and aluminum alloys are well known for their susceptibility to porosity formation during solidification. There are two main types of microporosity in castings: shrinkage porosity, which is due to the volume change upon solidification combined with restricted feeding of liquid in

*e-mail: alexandrefurtado@id.uff.br

the final solidification region, and gas porosity which is favored by dissolved gas in the melt upon high cooling rates, as a result of the difference in solubility between gases in the liquid and solid region. These microporosity manifest themselves in different ways in casting. They form in the mushy zone, and their morphologies and extent are distinct. Morphology of gas porosity, resembles a spherical shape, while shrinkage porosity morphology is almost always irregular and elongated[3].

Researches involving unidirectional solidification under transient heat flow for pure metals and their alloys have come into attention[4-15]. This technique allows the investigation of the solid/liquid surface morphology, microstructure and microsegregation as a function of the thermal parameters, which is very attractive for investigating the influence of these parameters in solidification of metals and alloys. According to the Silva et al.[4], the as-cast structures and microhardness obtained from upward transient directional solidification experiments with Al - 1.0 and 1.5 wt.% Fe alloys are strongly affected by solidification conditions. The experimental results showed that the microhardness can be correlated with Fe content of the alloy and cellular spacing. Ribeiro et al.[5] examined the solidification of Al-Fe alloys in the upward unidirectional solidification system. The focus of that study was to examine the influence of cell size and its intercellular phase distribution on the fatigue life. It was found that fatigue life decreases as cell spacing increases. Smaller cell spacing allows a homogeneous distribution of Al-Fe fibers within the intercellular regions, which tends to improve the fatigue property. Investigations proposed by Goulart et al.[6], have been made from solidification structure in Al-Fe alloys, which were directionally solidified under transient heat flow conditions. According to the authors, cellular microstructure prevailed along the entire castings for any alloy examined and cell spacing was strongly dependent of the thermal parameters such as cooling rate and solidification speed.

Avoiding unwanted properties in the castings, requires an understanding of the solidification behavior. So, the present work is elaborated in this general framework, emphasizing effects of the solidification conditions on the two of the types of defects found in the castings, such as microporosity and microsegregation. Since it is well known that aluminum alloys are susceptible to porosity formation and segregation during the solidification process.

2. Experimental Procedure

Al - 1.0 wt. % Fe alloy was prepared in an electrical resistance furnace at 750 ºC, from commercial purity metals, i.e., 99.9 wt % Al and 99.9 wt % Fe. The casting assembly used in the directional solidification experiments, which consists of water-cooled stainless steel mold with heat being extracted from the bottom, promoting vertical upward directional solidification process, Figure 1, more details on the casting assembly is presented by Ferreira et al.[10]. Solidification experiment was performed under thermally and solutally stable directional solidification conditions, i.e., natural convection due to density variations is not caused by temperature differences since the vertical casting is cooled from the mold bottom of stainless steel. The pouring temperature for Al - 1.0 wt. % Fe alloy
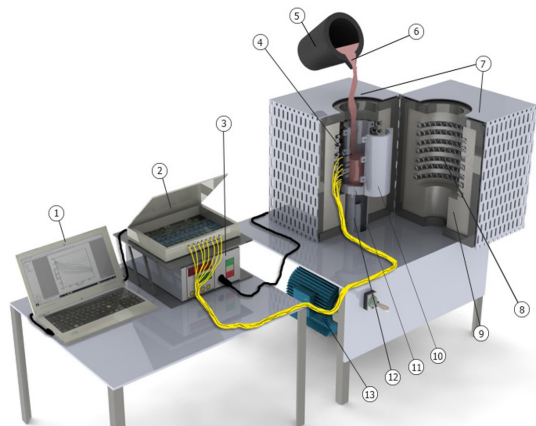
Figure 1. Diagrammatic representation of equipment: 1—Personal computer and data acquisition software; 2—Data logger hardware; 3—Temperature controller system; 4 — Type K thermocouples; 5 — Crucible; 6 — Melt; 7 — Unidirectional solidification furnace; 8 — Electric heaters; 9 — Ceramic fiber insulation; 10—Steel mold; 11—Steel plate; 12—Water cooling system; 13—Water pump.

was setup at 50 ^{0}C above the liquidus temperature. During solidification process, temperature data was collected by the output of a bank of type K thermocouples positioned at the central line of the casting at 5, 10, 15, 20, 35, 45, 60, 85 mm from the mold bottom. The cooling rate for Al – 1.0 wt. % Fe alloy has been experimentally determined considering the temperature vs. time data immediately after the passage of the liquidus temperature for the different thermocouples positions along the casting.

The temperature data were experimentally collected at very small intervals of 0.001 s, in order to permit an accurate determination of the thermal parameters. In order to ensure adequate solute concentration in alloy, concentration measurements for Fe solute were carried out via Optical Emission Spectrometer in samples extracted after experiment. After solidification experiment, the ingot was sectioned along its longitudinal direction and mechanically polished with abrasive papers and etched with an acid solution composed of 25 mL H_2O, 2.5 mL HF, 25 mL HNO_3; 60 mL HCl in order to reveal the macrostructure, Paradela et al.[11]. Selected transverse samples of the solidified casting extracted at different positions (from 5 to 85 mm) from the mold bottom were polished and etched with a solution of 0.5% HF in order to reveal the as-cast microstructure, according to Sales et al.[12]. A Nikon Eclipse Optical Microscope (LV150) was used to produce digital images that were analyzed using the NIS-Elements D software to measure the cellular spacings. Although electron microscopes (SEM) are powerful magnification tools with high-resolution images, for the dimensions involved in present work, the optical microscope was used since the obtained results did not justify the greater time and cost involved in the use of the electron microscopes. The schematic illustration of the cellular spacings measurements in the transverse sections are shown in Figure 2.

About 30 measurements were taken for different positions along casting, with local cellular spacing (λ_c) being equal to average value. The method adopted for measuring the cellular spacings (λ_c) for different positions in casting transverse section was the triangle method[13].

Microstructural Patterns, Microsegregation, Porosity, and Mechanical Properties of Hypoeutectic Al-Fe Alloy, and its Dependency with Solidification Thermal Parameters

3
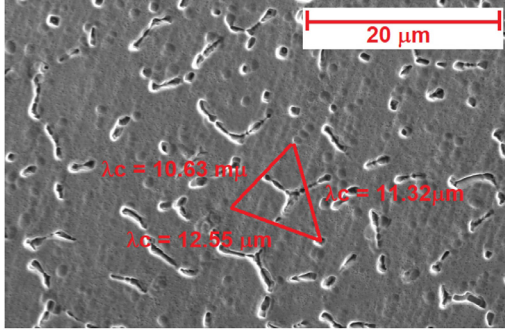
Figure 2. The schematic illustration of the cellular spacing (λ_C) measurements of an Al - 1.0 wt % Fe alloy sample.
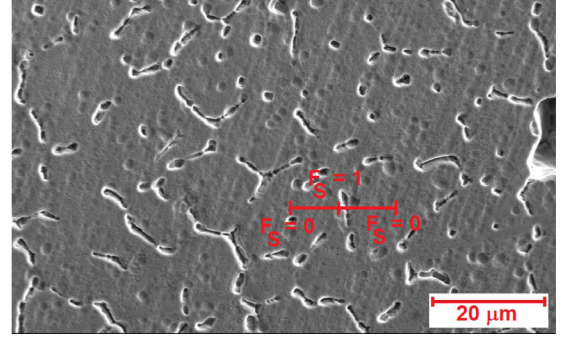
Figure 3. Representation of a track used for measurements of microsegregation profiles.

The measurements of microsegregation for Fe solute were taken with a scanning electron microscope JEOL in positions along the casting length. The concentration measurements of Fe are initiated at the center of cell ($F_S = 0$) and ended at the mid-point of the intercellular regions ($F_S = 1$), as shown in Figure 3. About 40 to 50 concentration measurements were performed for each examined position. Microsegregation profiles of Fe solute were determined in samples grown at solidification speed ranging from 0.45 to 1.0 mm/s.

According to Meza et al.[14] and Paradela et al.[15], the calculated results for microsegregation using the theoretical models (e.g., Scheil and Clyne–Kurz models) can yield discrepancies from the experimental data. In present work, we considered an experimental equation, in order to predict the Fe microsegregation. Experimental equation is based on a best-fit curve to the experimental microsegregation profiles, and is given by:

$$C_S = C_0 k_{ef} + a e^{b F_S} \qquad (1)$$

where C_0 represents initial concentration of Fe, F_S is solid fraction and "**a**" and "**b**" are experimental constants. Since the predict models using the equilibrium partition coefficient (k_{eq}) can yielded poor agreement between numerical and experimental results, we used an effective partition coefficient (k_{ef}) which takes into account the solidification speed. Burton et al.[16] proposed the follow equation for k_{ef}:

$$k_{ef} = \frac{k_{eq}}{k_{eq} + \left(1 - k_{eq} e^{\left(\frac{-S_S}{D_L}\right)}\right)} \qquad (2)$$

δ is the thickness of the diffusion boundary layer ahead the solidification interface and D_L represents Fe diffusivity in the liquid region. δ depends on the solidification speed (S_S), the liquid viscosity and agitation conditions ahead the solidification interface, and its value can vary from 10^{-6} to 10^{-3} m, Paradela et al.[15].

To characterize the area fraction of pores in the as-cast Al - 1.0 wt.% Fe alloy, all samples were cut in the transverse direction plane, from the bottom part of the mold to the

its top, mounted in conducting Bakelite, and polished to a 0.05 μm finish. Samples were analyzed using an EVO MA10 scanning electron microscope (SEM) equipped with a back-scattered electron (BSE) detector, and operated at 20 kV. Image threshold was applied to determine the porosity content (porosity %) using ImageJ Software[17], Figure 4.

Transverse samples were cut from the casting, as depicted in Figure 5, and prepared for tensile testing according to specifications of ASTM Standard E8M[18]. One transverse sample was cut from each position along casting, and prepared for tensile testing. Tensile tests were carried out with a speed of test equal to 3 mm.s^{-1}. The mechanical properties, i.e., ultimate tensile strength and elongation have been determined at different positions from casting base.

Microhardness test was carried out at room temperature using Leitz Wetzlar Microhardness Tester. Microhardness test was measured at least in 12 different regions on the transverse section, using a Vickers pyramidal indenter with a load and loading time of 100 g and 15 s, respectively, Figure 6.

3. Results and Discussion

Generally, solidification leads to two types of grain morphology; columnar and equiaxed. However, due to solidification processing conditions imposed by water cooled system, the structure known as columnar prevailed along the casting, i.e., no columnar to equiaxed transition has been observed and indicating that heat flux is unidirectionally oriented, Figure 7. However, it is well known that columnar to equiaxed transition is dependent on solidification conditions associated with the casting process, including superheat and solute content, Ferreira et al.[2] and Felipe et al.[19].

Figure 8 shows the phase diagram of the alloy system investigated, calculated by thermodynamics software[20] and emphasizing the liquid-solid transformation region. For Al – 1.0 wt% Fe alloy, according to the phase diagram the solidification begins at liquidus temperature of 657 °C and ends when it reaches the solidus temperature of 654 °C. Al – 1.0 wt% Fe alloy have a narrow solidification interval (3 °C), which minimizes the segregation during the solidification process. One can see that the point in phase diagram, which indicate chemical composition of 1.8 wt.% Fe and temperature equal to 654 °C, corresponding to the eutectic point. The maximum solid solubility of Fe in aluminum occurs at the eutectic temperature 654 °C and this solid
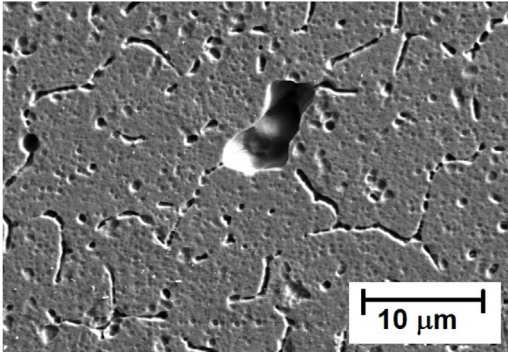
Figure 4. Image obtained from an EVO MA10 scanning electron microscope (SEM) of irregular shape porosity for Al - 1.0 wt.% Fe alloy.
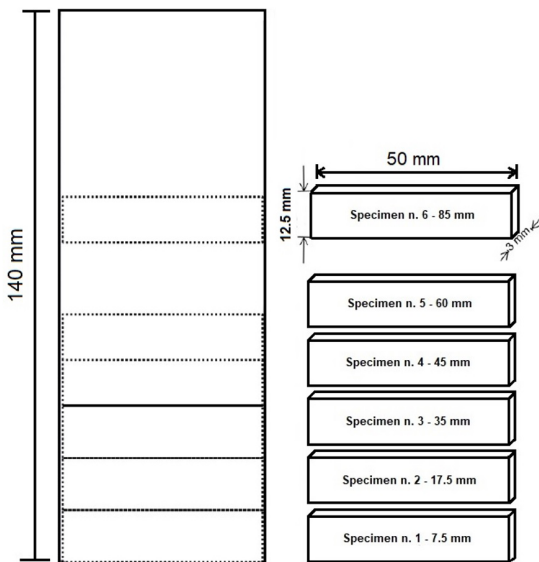
Figure 5. The schematic illustration for removal of specimens from the directionally solidified casting for tensile test.
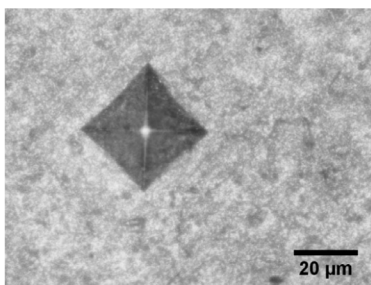
P = 85 mm

λ_C = 33.86 μm

H = 18.6 Hv

Figure 6. Indentation left in sample of the Al – 1.0 wt.% Fe alloy after Vickers microhardness test.

Figure 7. Directionally solidified macrostructure of hypoeutectic Al – 1.0 wt.% Fe alloy.
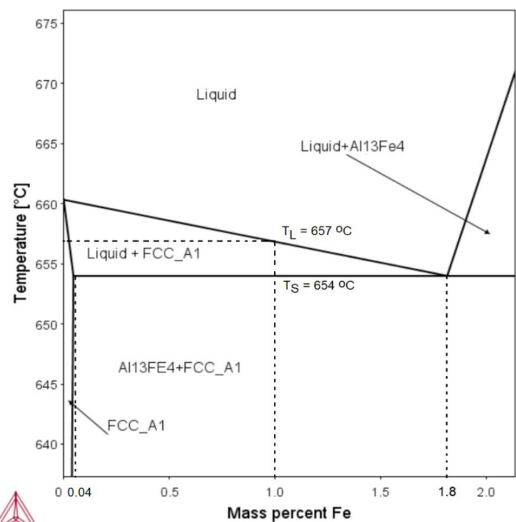
Figure 8. Phase diagram of Al-Fe system as computed with the Thermo-Calc Software[20] with Database TCBIN.

phase at this temperature has a composition of 0.04 wt.% Fe. Experiments focused on microsegregation; the equilibrium partition coefficient is calculated from equilibrium phase diagram. In the present paper, k_{eq} = 0.029 corresponds to the solute concentration ratio between the solid and liquid.

The cooling curve for hypoeutectic alloy, under slow solidification condition, i.e., no water-cooled solidification system, is depicted in Figure 9, in case analyzed the cooling rate was about 0.3 ºC/s. We can see in Figure 9, the corresponding experimental validation for the examined alloy, i.e., solidification begins at liquidus temperature of 657 ºC, as indicated by the change in the cooling curve caused by the latent heat release.

It is important to highlight that T_L is in agreement with observations from phase diagram, Figure 8. After solidification completion, the slope of cooling curves is again altered. In the other words, as material solidifies it releases its latent heat of fusion, holding the temperature precisely at its solidification temperature (T_L) until all the liquid is solid.

Microstructural Patterns, Microsegregation, Porosity, and Mechanical Properties of Hypoeutectic Al-Fe Alloy, and its Dependency with Solidification Thermal Parameters

5

Temperature profiles determined during the solidification process under transient heat flow conditions in a water-cooled solidification setup is shown in Figure 10.

To the right of Figure 10, information can be found concerning the position (**P**) in the ingot, values of passing time of liquidus and solidus temperatures. The temperature values are seen to decrease faster at regions closer to the water-cooled bottom. The cooling rate gradually dwindles toward completion of solidification. The experimental results of temperature versus time, presents a similar behavior with those found in the literature Sales et al.[12] and Paradela et al.[15]. From Figure 10, the position (**P**) of each thermocouple can be correlated with passing time of T_L. From this function (**P=f(t)**), the values of solidification speed (S_S) were found as a function of the time by computing the time derivative of **P**, Figure 11 display these results.

From experimental equation (**P=f(t)** and S_S**=f(t)**), it was possible to obtain an equation for solidification speed as function of position (S_S**=f(P)**), as shown in Figure 12. S_S is seen to decrease faster from the mold bottom, followed by a gradual decrease over length of casting. This is due to the fact that water cooling system favors higher solidification

speed close to mold bottom, which decreases along the casting because of the increase thermal resistance of the solidified layer. A comparative analysis of the profiles of the local solidification time (L_{ST}) and S_S versus **P**, reveal that S_S dwindles quickly in the regions very close to the mold bottom, followed by a gradual, slower decrease along the casting. One can see an inverse trend in the L_{ST} close to the bottom, L_{ST} increases faster; afterwards, it starts a gradual increase along the casting. High solidification speed favors a rapid solidification, i.e., a short local solidification time. It is worth mentioning that as-cast alloys with wide solidification intervals make them susceptible to microsegregation during the solidification process.

The thermal parameters, such as cooling rate ($\dot{T}$) and thermal gradient (**G**) for different positions, are shown in Figure 13.

Once again, the profiles of thermal parameters ($\dot{T}$ and **G**), indicate that both parameters are significantly affected by position of as-cast material, while preserving the same behavior along the casting length. These thermal parameters of solidification are key factors acting in parallel during the solidification experiment of hypoeutectic Al – 1.0 wt.% Fe alloy. These thermal parameters server to condition the changes not only on microstructural patterns itself (cells, dendrites, inclusions and porosity) but also the chemical arrangement (microsegregation), affecting the quality of the final product. It worth mentioning that the points in Figures 11, 12 and 13, are results obtained from the solidification experiment and the lines represents empirical power functions fit to the experimental points. Baptista et al.[7], Sales et al.[8] and Spinola and Spinelli[9], determined experimental expressions for both thermal parameters, which are similar to the showed in present work.

Typical cellular microstructure can be observed along the transverse sections of the as-cast alloy directionally solidified, Figure 14. Despite the relatively high cooling rates imposed by the water-cooled system during the directional solidification, cellular microstructures were predominant in Al – 1.0 wt.% Fe alloy.

Effect of thermal parameters (S_S, $\dot{T}$ and L_{ST}) on the cellular spacing is depicted in Figure 15. This influence translates to the change in cellular spacing (λ_C), i.e., high values of S_S and
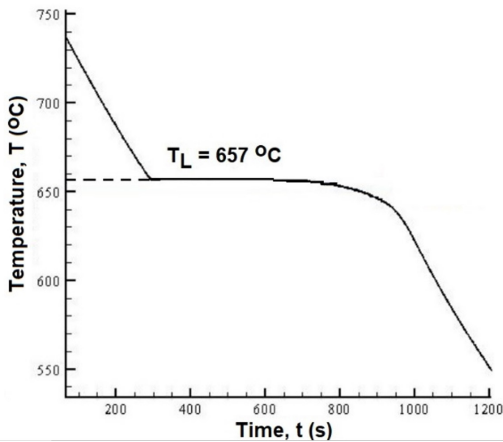
Figure 9. Experimental cooling curves of hypoeutectic Al – 1.0 wt.% Fe alloy.

Position,	T_L	T_S
P (mm)	Time, t (s)	Time, t (s)
5	8.76	10.37
10	15.34	17.94
15	22.65	25.93
20	30.24	34.50
35	59.27	64.21
45	76.15	82.10
60	123.86	131.23
85	185.10	195.18
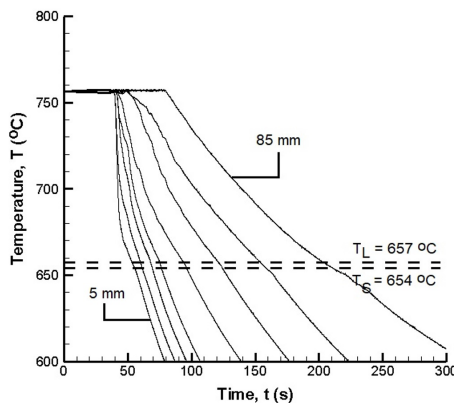
Figure 10. Temperature versus time.
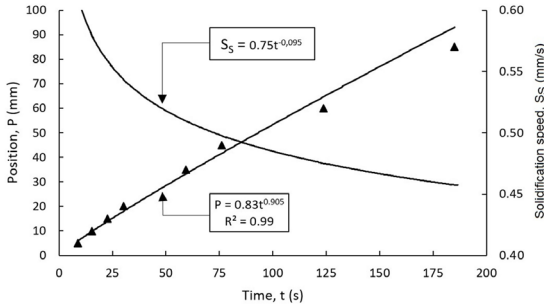
Figure 11. Position (**P**) and solidification speed (S_S) as a function of time (**t**).
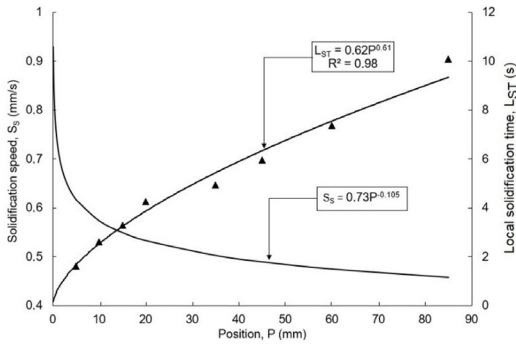
Figure 12. Solidification speed (S_S) and local solidification time (L_{ST}) as a function of position (**P**).
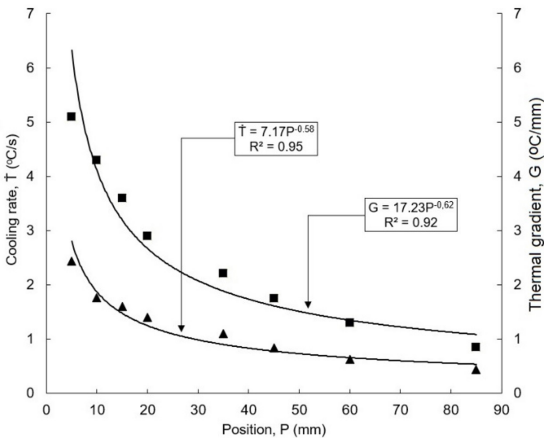
Figure 13. Cooling rate ($\dot{T}$) and thermal gradient (**G**) as a function of position (**P**).

$\dot{T}$ (P = 5 mm) near the mold bottom, favors a more refined microstructure and low values of said thermal parameters close to the top of the casting, contribute effectively to a coarser microstructure, Figure 15b and 15c. In contrast, an inverse behavior can be observed from the λ_C versus L_{ST}, lower L_{ST} found close to mold bottom (P = 5 mm), favors a decrease in the λ_C. However, as the L_{ST} increase, one can see also a continuous increase of λ_C. From the analysis of these experimental data, it can be concluded that the increase in the

S_S and $\dot{T}$ reduce the possibility of the cellular growth during the solidification experiment, through decreasing the L_{ST}.

Considering that our solidification experiment of Al – 1.0 wt.% Fe alloy has been carried out with non-equilibrium conditions, it was necessary to monitor the microsegregation profiles under high solidification speeds. First of all, Burton's equation (Equation 2) has been used to create a graph of effective partition coefficient (k_{ef}) versus solidification speed (S_S). In order to found an experimental equation for k_{ef}, a curve fitting technique was used on the experimental points, as shown in Figure 16.

We can see in Figure 16 that k_{ef} has been calculated for a range of solidification speed between 0.46 to 0.62 mm/s. For higher solidification speeds there is a tendency to $k_{ef} = 1$ and for lower speeds the k_{ef} will be equal to k_{eq}, since this empirical equation is operative in the range $k_{eq} < k_{ef} < 1$. To understand the chemical arrangement during the solidification experiment, the microsegregation profiles were experimentally measured along the casting length. Figure 17 depicts the measured microsegregation profiles along the microsegregation path, taken from the center of cell (**F = 0**) to the mid-point of the intercellular region (**F = 1**), as previously discussed. Predictions of empirical equation (Equation 1) with k_{ef}, are plotted in this same Figure, for comparison purposes. The empirical equation with experimental constants fitted to the microsegregation profiles for different positions in casting, are listed in Table 1. As expected, in any cases analyzed, it can be seen that the Fe concentration increases with solidified fraction. One can see from Figure 17, that microsegregation profiles (curves and experimental data) move upward with the increase in S_S and decrease in **P**, which indicates that solubility of Fe solute increases with the increase in S_S. This occurs due to the solidification experiment under high speeds and Fe solute slowly diffusing in the liquid region, can lead increasing levels of the Fe content in this liquid region close to solidification front, this in turn, correspondingly increase the Fe content in the solid region along the microsegregation path. That results are in agreement with effect of solidification speed on microsegregation on aluminum alloys reported in Refs[11,14].

It can be seen from Figure 17 that the empirical equation has an excellent agreement with the experimental data for the entire range of solid fractions (F_S) and solidification speeds (S_S). The predicted concentration of Fe by the empirical equation, from the cell cores ($F_S = 0$) to the intercellular regions ($F_S = 1$) adjusted well to the experimental profiles.

According to Meza et al.[14], the experimental constant "**a**" seems to depend on the considered alloy system, which was adjusted to be 0.03 for hypoeutectic Al – 1.0 wt.% Fe alloy. However, the experimental constant "**b**" seems to be associated with the solidification speed, i.e., for a given alloy system, it increases with the increase in solidification speed (S_S), as shown in Table 1.

It is well known that quality of the final product depends to a large extent on soundness of the aluminum alloys casting, in which the porosity content is to be minimized. Aluminum alloys are known for their susceptibility to porosity formation during solidification. According to the literature[21-25], thermal parameters can to influence behavior of the castings during

Microstructural Patterns, Microsegregation, Porosity, and Mechanical Properties of Hypoeutectic Al-Fe Alloy, and its Dependency with Solidification Thermal Parameters

7

P = 15 mm

S_S = 0.55 mm/s

L_{ST} = 3.28 s

$\dot{T}$ = 1.6 ºC/s

G = 3.6 ºC/mm

λ_C = 20.00 µm

P = 35 mm

S_S = 0.50 mm/s

L_{ST} = 4.94 s

$\dot{T}$ = 1.1 ºC/s

G = 2.2 ºC/mm

λ_C = 23.21 µm

P = 85 mm

S_S = 0.46 mm/s

L_{ST} = 10.08 s

$\dot{T}$ = 0.4 ºC/s

G = 0.8 ºC/mm

λ_C = 33.86 µm
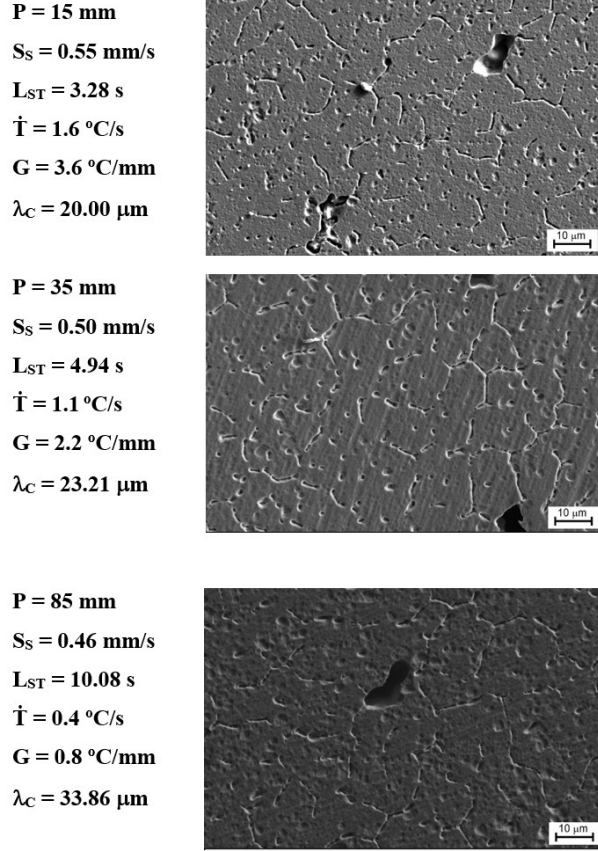
Figure 14. Typical cellular microstructure of samples taken from transverse sections along the casting of the hypoeutectic Al – 1.0 wt.% Fe alloy.

Table 1. Experimental equation determined from best-fit curve to the experimental data.

$C_S = C_o.k_{ef} + a.exp^{(b.F_S)}$			
Position, P (mm)	5	15	35	60
Solidification speed, S_S (mm/s)	0.69	0.58	0.50	0.45
Effective partition coefficient, k_{ef} (-)	0.69	0.58	0.50	0.24
experimental constant, a (-)	0.03	0.03	0.03	0.03
experimental constant, b (-)	4.89	4.67	4.27	4.33

the solidification process, and still combination of those parameters or even castings geometry. One of the purposes of the present experimental work, was to study the thermal parameters effect on porosity formation in Al - 1.0 wt.% Fe alloy obtained from vertical upward directional solidification process. Figure 18a-c shows micrographs obtained from the scanning electron microscope (SEM), taken at heights corresponding to where the thermocouples were located.

By considering the micrographs presented in Figure 18, we can to conclude that the two main causes of porosity were found during solidification experiment: a) Shrinkage porosity, due to the volume change upon solidification, and b) Gas porosity, due to the dissolved gases in the melt upon freezing. Also, one can see a slight increase in the size of porosity with increasing distance from the water-cooled

bottom, these results are consistent with those found by Lashkari et al.[23].

The relationship between thermal parameters and porosity content is depicted in Figure 19.

Figure 19a shows the relationship between the porosity content determined from the analysis-based on ImageJ Software[17] and positions (**P**) where the thermocouples were positioned during solidification experiment. One can see that porosity content increases clearly with increasing position (**P**). This dependence on position along casting, is related to the fact that the upward directional solidification technique allows wide ranges of thermal parameters (S_S, $\dot{T}$ and L_{ST}) during experiment. The solidification apparatus with water-cooled mold is useful when high rates of heat extraction to be achieved. A curve fitting technique from the experimental
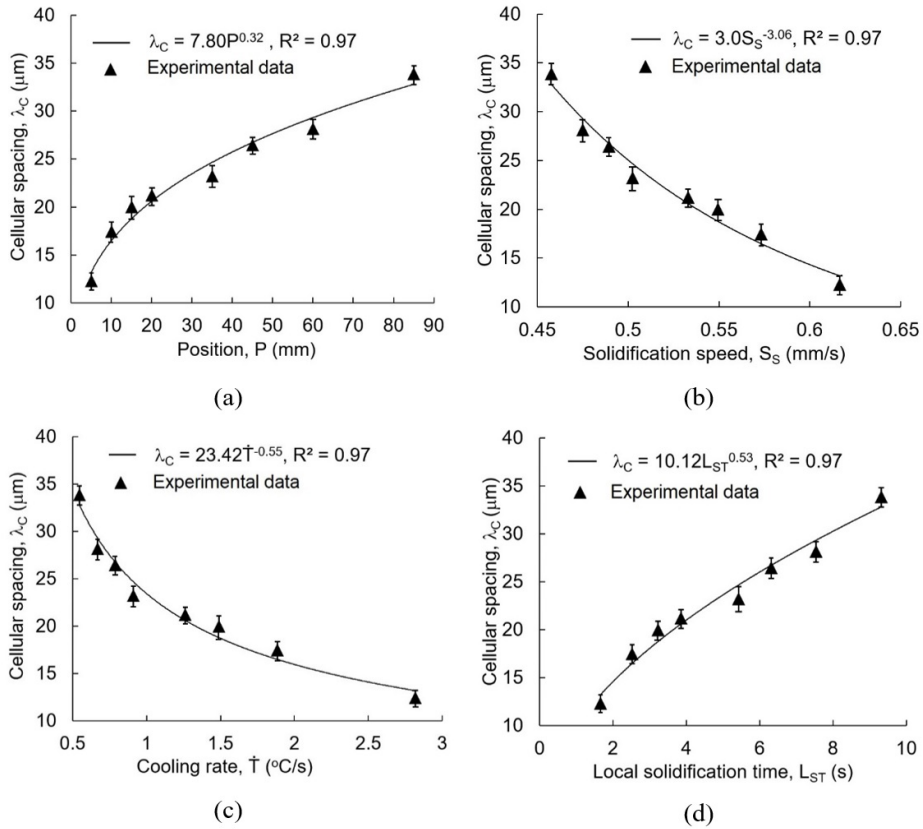
Figure 15. Cellular spacing (λ_C) versus: a) Position (P) in the casting, b) Solidification speed (S_S), c) Cooling rate ($\dot{T}$), and d) Local solidification time (L_{ST}).

points has generated power functions, in order to represent the effect of solidification thermal parameters on the porosity content. The porosity content decreases significantly with increasing solidification speed (Figure19b) and with cooling rate (Figure19c). However, experimental results of porosity versus L_{ST} present an inverse behavior to the those found from the S_S and $\dot{T}$, i.e., porosity content increases with L_{ST}, (Figure19d). The two fundamental effects that contribute to the formation of porosity during solidifying alloys, are the shrinkage resulting from the volume decrease in going from liquid to solid, and gas evolution resulting from the decrease in solubility in solid region compared to the liquid. Both phenomena found in present work, can occur simultaneously and act synergistically to develop porosity during casting. When the aluminum alloy solidifies, solubility of hydrogen in the liquid is decreased and gas porosities can be formed. When water-cooled mold system is applied, high solidification speed, high cooling rates and short local solidification time are obtained close to the mold bottom and gas in this region is supersaturated. This avoids nucleation of gas porosity, so content of gas porosity can be minimized, Figure 19b-d. The water-cooled system, as previously discussed, are usually used to optimize the thermal parameters, and have several advantages as increase of temperature gradient, decrease of local solidification time, finer grain structure, decrease of cellular or dendrite spacing and decrease of shrinkage cavities. So, it is to be expected that higher solidification
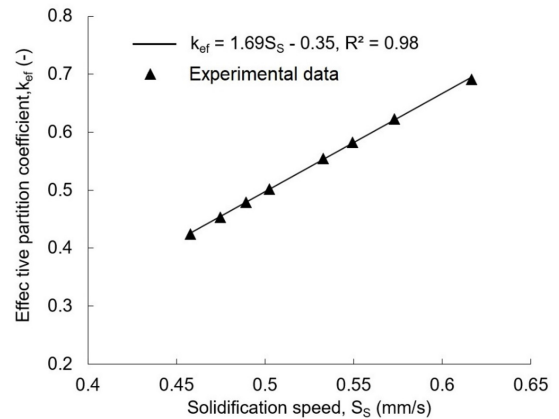
Figure 16. Effective partition coefficient (k_{ef}) as a function of solidification speed (S_S).

speeds and high cooling rates close to the mold bottom, also favors decrease in shrinkage porosity. Since the thermal parameters depend on the position in the casting, the values of porosity content also vary in the distribution of these thermal parameters proportionally, Figure 19b-d.

Next, the relationships between mechanical properties (ultimate tensile strength, elongation and microhardness)

Microstructural Patterns, Microsegregation, Porosity, and Mechanical Properties of Hypoeutectic Al-Fe Alloy, and its Dependency with Solidification Thermal Parameters

9

with solidification thermal parameters, cellular spacing and porosity content are presented and discussed. Figure 20 depicts relationship between ultimate tensile strength (σ_U) and cooling rate ($\dot{T}$), local solidification time (L_{ST}), cellular spacing (λ_C) and porosity content (P_C). One can see in Figure 20, both higher cooling rates (Figure 20a) and a short local solidification time (Figure 20b) favors ultimate tensile strength. According to Goulart et al.[6], tensile strength seems to be closely related with the intermetallic phases (Al$_3$Fe/

Al$_6$Fe) and cellular spacings (Figure 20c), which in turn, are associated to the solidification processing parameters. High cooling rates (Figure 20a) with a short solidification time (Figure 20b) can induce the finely dispersed intermetallic phases and most refined microstructure, as consequence, the ultimate tensile strength is correspondly increased. Indeed, ultimate tensile strength increases its value from 59.4 MPa with a cooling rate equal to 0.54 ℃/s to 70 MPa for a cooling rate of about 1.88 ℃/s, Figure 20a. The tensile tests result of Al - 1.0 wt. %Fe alloy, have shown that strength increased in 18% at the position of 10 mm when compared with tensile strength found from position of 85 mm. Porosity content in cast material has been known as a defect affecting the enhancement of tensile strength. The porosity content, in turn, is affected by casting parameters, such as cooling rate and local solidification time. Optimum mechanical properties, e.g., ultimate tensile strength is attained with least porosity content, as shown in Figure 20d. The most probable cause of dependence of strength on the porosity content, can be attributed to failures initiated from the pores within the cast material.

High cooling rates and shorter local solidification time favors ultimate tensile strength, Figure 20a and 20b, similar behavior is found for the elongation of Al - 1.0 wt.% Fe alloy, Figure 21a and Figure 21b. In the elongation case, the influence of cellular spacing is negative, i.e.,
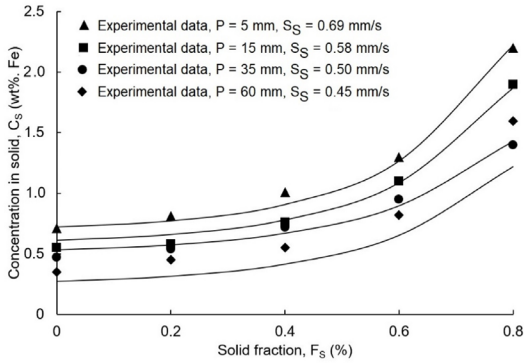
Figure 17. Effect of solidification speed (S_s) on the microsegregation profile at different positions (**P**) along the casting length.

(a)

(b)

(c)
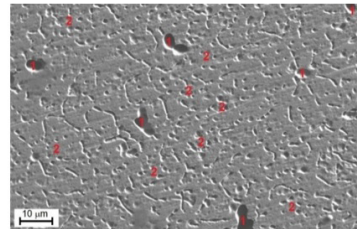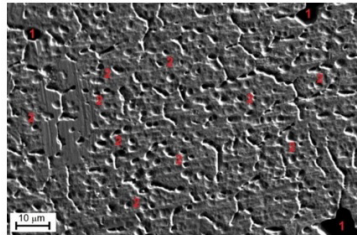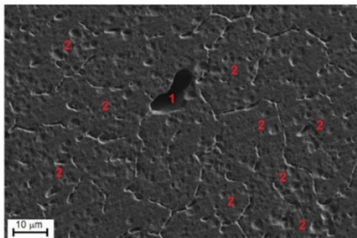
Figure 18. Porosity as observed by scanning electron microscopy (SEM) in Al – 1.0 wt.% Fe alloy, at different distance from the water-cooled bottom: a) 10 mm; b) 20 mm, and c) 85 mm.
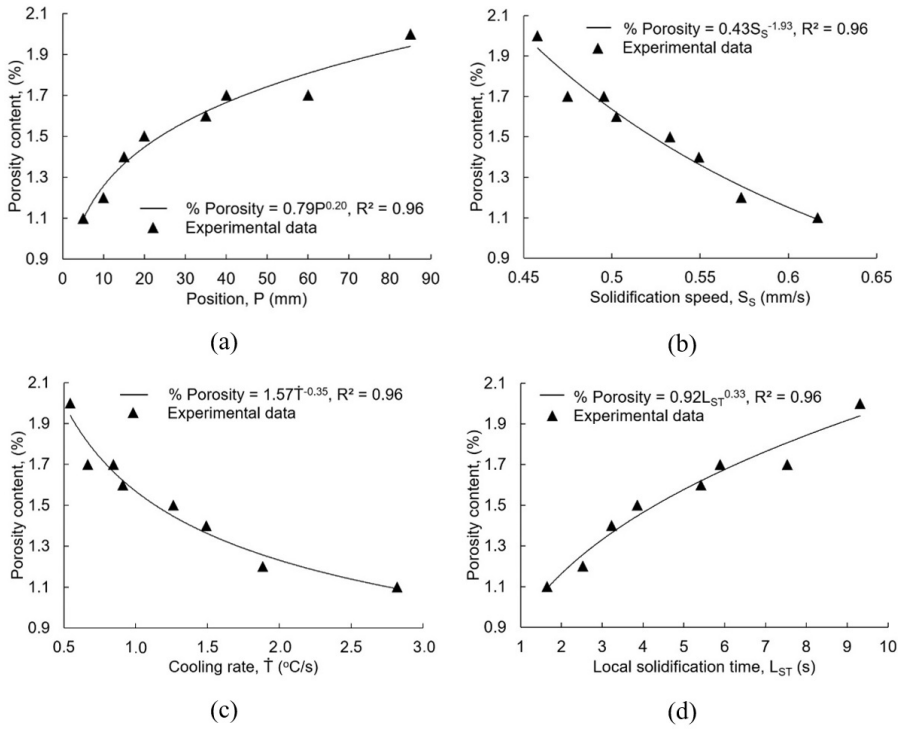
Figure 19. Porosity content versus a) Position (**P**) in the casting, b) Solidification speed (**S$_s$**), c) Cooling rate (**Ṫ**), and d) Local solidification time (**L$_{ST}$**).
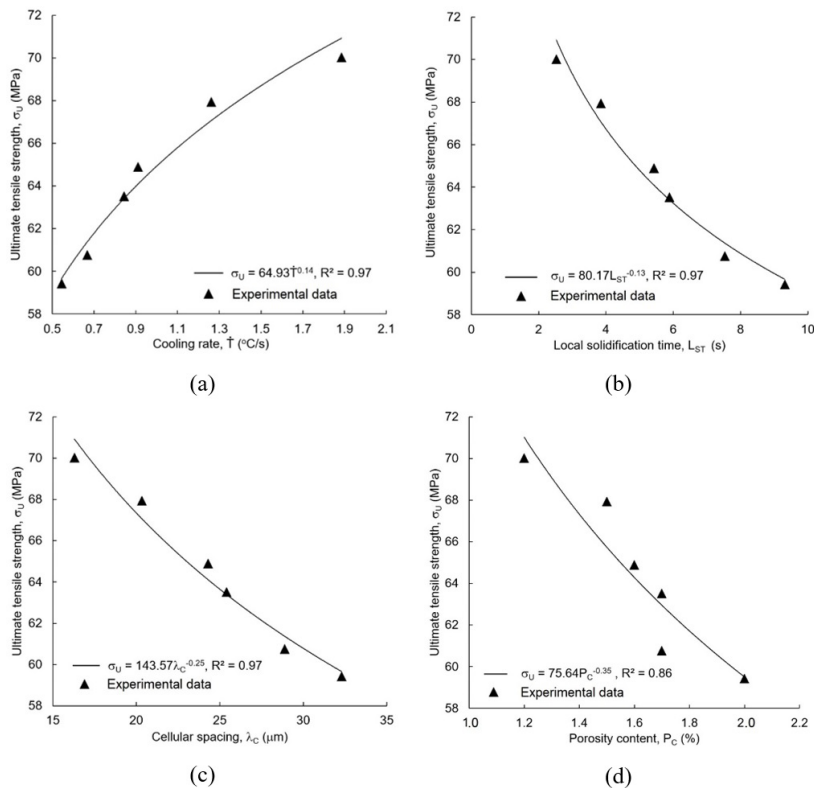
Figure 20. Ultimate tensile strength (σ_U) versus: a) Cooling rate (Ṫ); b) Local solidification time (L$_{ST}$); c) Cellular spacing (λ_C); and d) Porosity content (**P$_C$**).
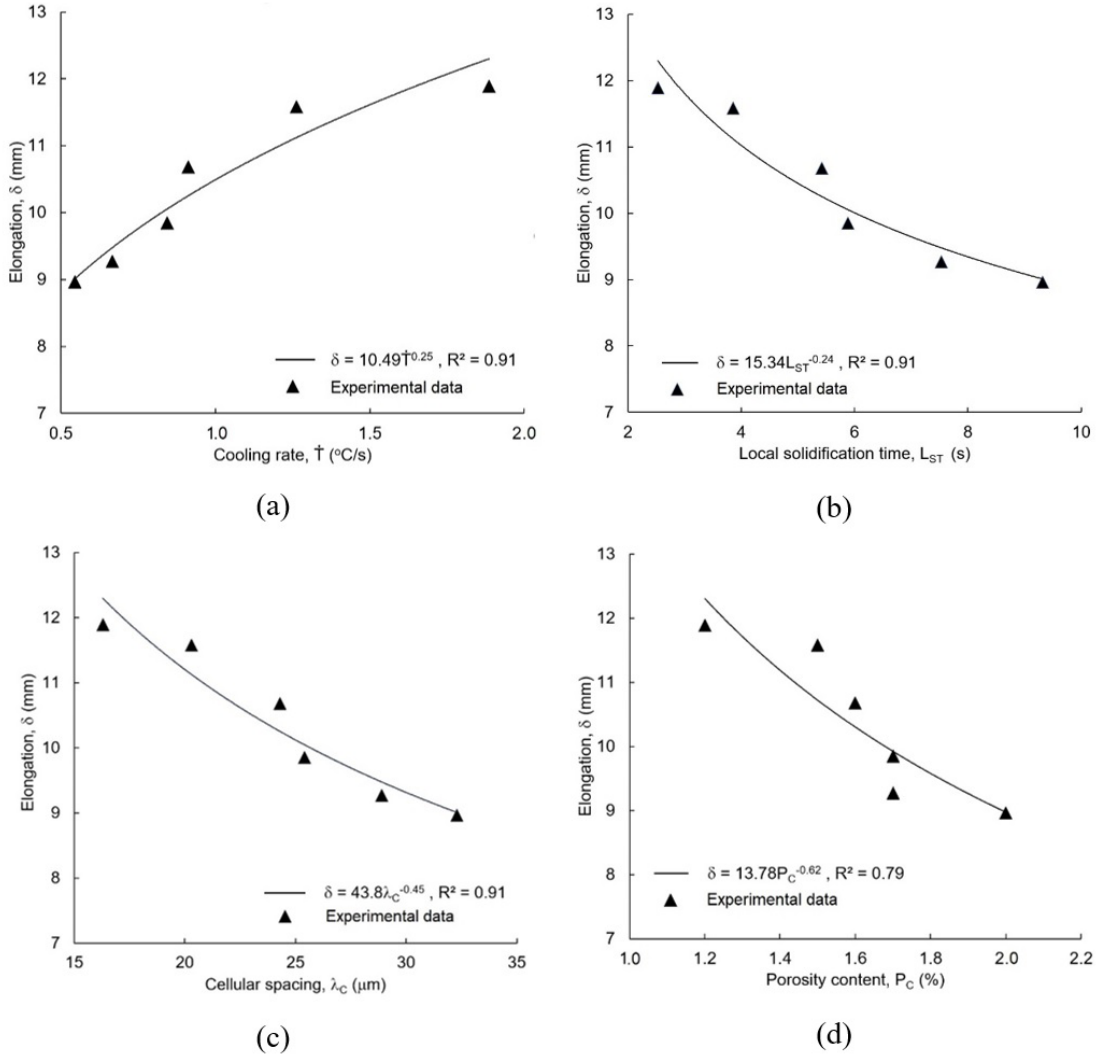
Figure 21. Elongation (δ) versus: a) Cooling rate ($\dot{T}$); b) Local solidification time (L_{ST}); c) Cellular spacing (λ_C); and d) Porosity content (P_C).

higher cellular spacing tends to decrease this mechanical property, Figure 21c. When the microstructural spacing is increased, coarser Al₃Fe is formed, contributing to the nucleation of fissures. In the regions characterized by coarser microstructure found close to the top mold, such damage can be even more intense. As a consequence, the Al - 1.0 wt.% Fe alloy presented lower ductility when compared to the other positions close to the bottom mold. Porosity also significantly affects elongation of the as-cast Al - 1.0 wt.% Fe alloy. The lower elongations found in as-cast alloy, can be attributed to the presence of higher porosity content, as shown in Figure 21d. Porosity content, pore size/shape, and its spacing are important factors that control the elongation of the material, which in turn, is one way to measure and quantify the ductility of the as-cast alloys.

Effects of the thermal parameters, cellular spacing and porosity content on the microhardness, also are highlighted in present paper, Figure 22. Once again, one can see that high

cooling rates (Figure 22a) and very short solidification time (Figure 22b) favored m0icrohardness, similar results also were found by Felipe et al.[19]. The results of microhardness versus cellular spacings (λ_C) are shown in Figure 22c. Microhardness after unidirectional vertical solidification, analyzed in present work, is proved to decrease with increase cellular spacings. As expected, in positions near the mold bottom, an improvement in microhardness is observed, due to the finer microstructure as a consequence of high values of cooling rate and short solidification time. As shown in Figure 21c, the microhardness decreased from 35.2 to 18.6 HV, which confirms a reduction of 47%. Figure 22d reveals that presence of higher porosity contents, i.e., from 1.1% at the position of 5 mm to 2.0% at the position of 85 mm, decreased the microhardness of as-cast alloy, from 35.2 HV to 18.6 HV. The presence of high porosity content decreases the microhardness, due primarily to the failure process is initiated from the voids formed within the as-cast alloy.
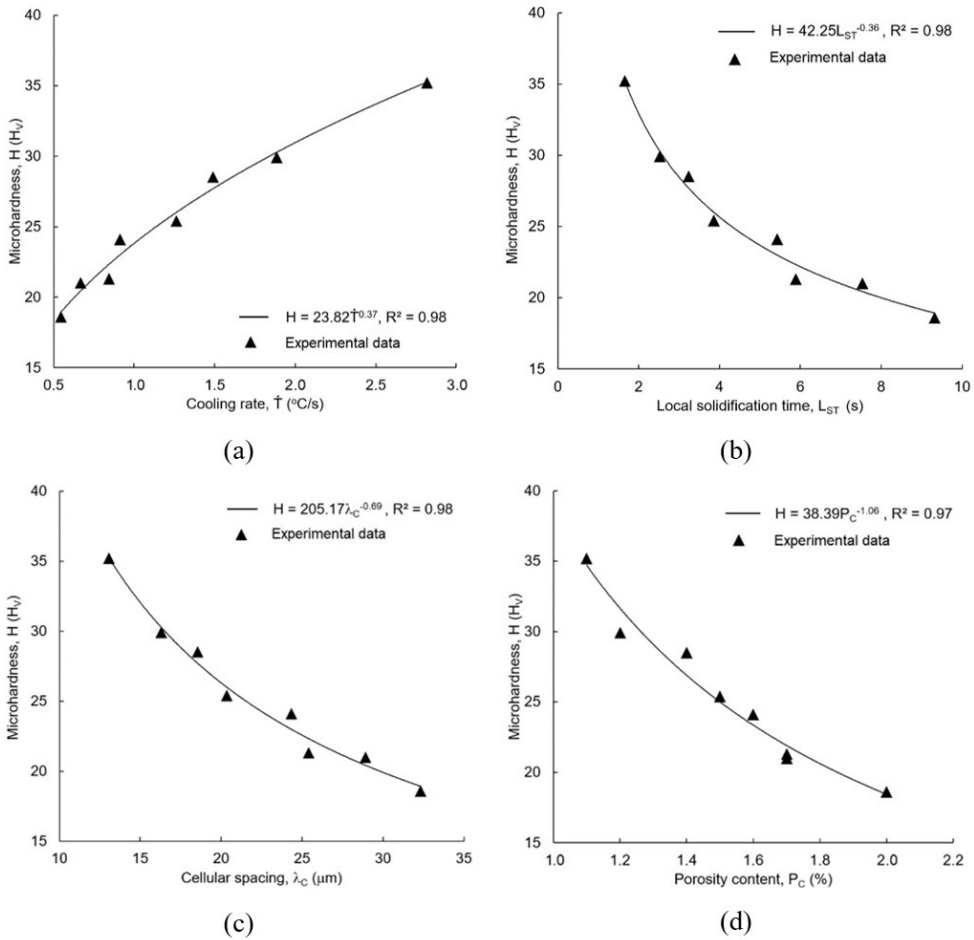
Figure 22. Microhardness (**H**) versus: a) Cooling rate ($\dot{\mathrm{T}}$); b) Local solidification time ($\mathbf{L_{ST}}$); c) Cellular spacing (λ_C); and d) Porosity content ($\mathbf{P}_C$).

4. Conclusions

The results herein represent a response to information required concerning the influence of solidification thermal parameters on the microstructural patterns, microsegregation, porosity, and mechanical properties of a hypoeutectic Al-Fe alloy. Due to solidification processing conditions considered during experiment, the columnar morphology prevailed along the entire ingot. High solidification speed, cooling rate, thermal gradient and a very short local solidification time were found in regions close to the mold bottom. The presence of a water-cooled system favored these results. Farther away from the mold bottom, one can observe an inverse behavior of the thermal parameters, because of the increased thermal resistance of the solidified region. These changes in thermal parameters along the casting, served to condition the changes not only on cellular spacing, but also the microsegregation, porosity and mechanical properties of the as-cast alloy. This influence translated to the changes in cellular spacing, i.e., a more refined microstructure in regions close to the mold bottom and a coarser microstructure for the regions near to the top. An experimental equation determined from best-fit curve to the experimental data of microsegregation was considered. The good agreement between results is due to effective partition coefficient considered in equation. This coefficient, in turn, was experimentally determined for a range of solidification speed between 0.46 to 0.62 mm/s.

Experimental results obtained from porosity content, have pointed out that the its value increases with position along the ingot. This dependence on the position, is related to the fact that upward directional solidification system allows wide ranges of thermal parameters. Since the parameters depend on the position in the casting, the values of porosity content also vary with distribution of these thermal parameters, proportionally.

Through an analysis of the experimental data for mechanical properties, it can be concluded that ultimate tensile strength, elongation and microhardness resulting from experiment, are closely related to the solidification processing parameters and porosity of the as-cast alloy.

This work provides an understanding to the thermal parameters obtained during upward transient directional solidification of Al-Fe alloy, and an overview of its effects on the as-cast alloy.

5. Acknowledgments

6. References

1. Dutta B, Rettenmayr M. Effect of cooling rate on the solidification behavior of Al–Fe–Si alloys. Mater Sci Eng A. 2000;283(1-2):218-24. http://dx.doi.org/10.1016/S0921-5093(00)00742-5.

2. Ferreira AF, Chrisóstimo WB, Sales RC, Garção WJL, Sousa NP. Effect of pouring temperature on microstructure and microsegregation of as-cast aluminum alloy. Int J Adv Manuf Technol. 2019;104(1-4):957-65. http://dx.doi.org/10.1007/s00170-019-03979-6.

3. Cao F, Li H, Ning Z, Jia Y, Gu X, Yu L, et al. The formation mechanism of porosity for spray-deposited 7075 alloy. Mater Res. 2015;18(Suppl. 1):89-94. http://dx.doi.org/10.1590/1516-1439.328414.

4. Silva BL, Garcia A, Spinelli JE. The effects of microstructure and intermetallic phases of directionally solidified Al–Fe alloys on microhardness. Mater Lett. 2012;89:291-5. http://dx.doi.org/10.1016/j.matlet.2012.08.130.

5. Ribeiro PL, Silva BL, Silva WS, Spinelli JE. Effects of cellular growth on fatigue life of directionally solidified hypoeutectic Al-Fe alloys. Mater Res. 2014;17(3):767-74. http://dx.doi.org/10.1590/S1516-14392014005000021.

6. Goulart PR, Cruz KS, Spinelli JE, Ferreira IL, Cheung N, Garcia A. Cellular growth during transient directional solidification of hypoeutectic Al–Fe alloys. J Alloys Compd. 2009;470(1-2):589-99. http://dx.doi.org/10.1016/j.jallcom.2008.03.026.

7. Baptista LAS, Paradela KG, Ferreira IL, Garcia A, Ferreira AF. Experimental study of the evolution of tertiary dendritic arms and microsegregation in directionally solidified Al–Si–Cu alloys castings. J Mater Res Technol. 2019;8(1):1515-21. http://dx.doi.org/10.1016/j.jmrt.2018.05.021.

8. Sales RC, Ferreira LO, Almeida RP, Terra BP, Moura LJ, Ferreira AF. Microstructure and microhardness of directionally solidified Al-Si alloys subjected to an equal-channel angular pressing process. Mater Res. 2022;25:e20210344. http://dx.doi.org/10.1590/1980-5373-mr-2021-0344.

9. Spinola TS, Spinelli JE. Transient directional solidification of cast iron: microstructure formation, columnar to equiaxed transition and hardness. Mater Res. 2016;19(4):795-801. http://dx.doi.org/10.1590/1980-5373-MR-2015-0777.

10. Ferreira AF, Ferreira IL, Almeida RP, Castro JA, Sales RC, Junior ZA. Microstructural evolution and microsegregation in directional solidification of hypoeutectic Al−Cu alloy: a comparison between experimental data and numerical results obtained via phase-field model. Trans Nonferrous Met Soc China. 2021;31(7):1853-67. http://dx.doi.org/10.1016/S1003-6326(21)65622-4.

11. Paradela KG, Baptista LAS, Sales RC, Felipe PF Jr, Ferreira AF. Investigation of thermal parameters effects on the microstructure, microhardness and microsegregation of Cu-Sn alloy directionally

12. solidified under transient heat flow conditions. Mater Res. 2019;22(4):e20190259. http://dx.doi.org/10.1590/1980-5373-mr-2019-0259.

12. Sales RC, Felipe P Jr, Paradela KG, Garção WJL, Ferreira AF. Effect of solidification processing parameters and silicon content on the dendritic spacing and hardness in hypoeutectic Al-Si alloys. Mater Res. 2018;21(6):e20180333. http://dx.doi.org/10.1590/1980-5373-mr-2018-0333.

13. Silva BL, Garcia A, Spinelli JE. The effects of microstructure and intermetallic phases of directionally solidified Al–Fe alloys on microhardness. Mater Lett. 2012;89:291-5. http://dx.doi.org/10.1016/j.matlet.2012.08.130.

14. Meza ES, Bertelli F, Goulart PR, Cheung N, Garcia A. The Effect of the growth rate on microsegregation: experimental investigation in hypoeutectic Al–Fe and Al–Cu alloys directionally solidified. J Alloys Compd. 2013;561:193-200. http://dx.doi.org/10.1016/j.jallcom.2013.01.180.

15. Paradela KG, Garção WJL, Baptista LAS, Sales RC, Oliveira VC, Ferreira AF. The effect of the cooling rate on the microstructure and microsegregation: an experimental and numerical investigation of solidification in hypoperitectic Cu − 20 wt.% Sn alloy. Mater Res. 2020;23(4):e20200110. http://dx.doi.org/10.1590/1980-5373-mr-2020-0110.

16. Burton JA, Prim RC, Slichter WP. The distribution of solute in crystals grown from the melt. Part I. Theoretical. J Chem Phys. 1953;21(11):1987-90. http://dx.doi.org/10.1063/1.1698728.

17. Rasband W. ImageJ [Internet]. Bethesda: U.S. National Institutes of Health; 2014 [cited 2022 Apr 6]. Available from: http://imagej.nih.gov/ij

18. ASTM: American Society for Testing and Materials. ASTM E8M: standard test methods for tension testing of metallic materials. West Conshohocken: ASTM; 1995.

19. Felipe P Jr, Ferreira LO, Garção WJL, Almeida RP, Melo CM, Ferreira AF. Heat-flow parameters affecting microstructure and mechanical properties of Al–Cu and Al–Ni alloys in directional solidification: an experimental comparative study. Int J Mater Res. 2022;113(3):181-93. http://dx.doi.org/10.1515/ijmr-2020-8146.

20. Thermo-Calc Software AB. Thermo-Calc. Sweden.

21. Sigworth G, Wang C. Mechanisms of porosity formation during solidification: a theoretical analysis. Metall Trans, B, Process Metall. 1993;24(2):349-64. http://dx.doi.org/10.1007/BF02659138.

22. Casolco SR, Dominguez G, Sandoval D, Garay JE. Processing and mechanical behavior of Zn–Al–Cu porous alloys. Mater Sci Eng A. 2007;471(1-2):28-33. http://dx.doi.org/10.1016/j.msea.2007.03.009.

23. Lashkari O, Yao L, Cockcroft S, Maijer D. X-Ray microtomographic characterization of porosity in aluminum alloy A356. Metall Mater Trans, A Phys Metall Mater Sci. 2009;40(4):991-9. http://dx.doi.org/10.1007/s11661-008-9778-9.

24. Bhagavath S, Cai B, Atwood R, Li M, Ghaffari B, Lee PD, et al. Combined deformation and solidification-driven porosity formation in aluminum alloys. Metall Mater Trans, A Phys Metall Mater Sci. 2019;50(10):4891-9. http://dx.doi.org/10.1007/s11661-019-05378-8.

25. Kuo YS. Study of solidification time and solidus velocity on porosity formation in high strength aluminum alloy castings. Appl Mech Mater. 2014;575:442-5. http://dx.doi.org/10.4028/www.scientific.net/AMM.575.442.